ACS APPLIED MATERIALS & INTERFACES

Research Article

www.acsami.org

# Solution-Processed $MoO_3$:PEDOT:PSS Hybrid Hole Transporting Layer for Inverted Polymer Solar Cells

Yiling Wang,[†,§] Qun Luo,*[,†] Na Wu,[†] Qiankun Wang,[ξ] Hongfei Zhu,[‡] Liwei Chen,[‡] Yan-Qing Li,[ξ] Liqiang Luo,[§] and Chang-Qi Ma*[,†]

[†]Printable Electronics Research Center, Suzhou Institute of Nano-Tech and Nano-Bionic, Chinese Academy of Sciences, Suzhou, 215123, P. R. China

[‡]i-Lab, Suzhou Institute of Nano-Tech and Nano-Bionic, Chinese Academy of Sciences, Suzhou, 215123, P. R. China

[§]Department of Chemistry, Shanghai University, Shanghai, 200444, P. R. China

[ξ]Institute of Functional Nano & Soft Materials, Soochow University, Suzhou, 215123. P. R. China

Supporting Information

**ABSTRACT:** Solution-processed organic−inorganic hybrids composing of $MoO_3$ nanoparticles and PEDOT:PSS were developed for use in inverted organic solar cells as hole transporting layer (HTL). The hybrid $MoO_3$:PEDOT:PSS inks were prepared by simply mixing PEDOT:PSS aqueous and $MoO_3$ ethanol suspension together. A core−shell structure was proposed in the $MoO_3$:PEDOT:PSS hybrid ink, where PEDOT chains act as the core and $MoO_3$ nanoparticles connected with PSS chains act as the composite shell. The mixing with PEDOT:PSS suppressed the aggregation of $MoO_3$ nanoparticles, which led to a smoother surface. In addition, since the hydrophilic PSS chains were passivated through preferentially connection with $MoO_3$, the stronger adhesion between $MoO_3$ nanoparticles and the photoactive layer improved the film forming ability of the $MoO_3$:PEDOT:PSS hybrid ink. The $MoO_3$:PEDOT:PSS hybrid HTL can therefore be feasibly deposited onto the hydrophobic photoactive polymer layer without any surface treatment. The use of the $MoO_3$:PEDOT:PSS hybrid HTL resulted in the optimized P3HT:$PC_{61}$BM- and PTB7:$PC_{61}$BM-based inverted organic solar cells reaching highest power conversion efficiencies of 3.29% and 5.92%, respectively, which were comparable with that of the control devices using thermally evaporated $MoO_3$ HTL (3.05% and 6.01%, respectively). Furthermore, less HTL thickness dependence of device performance was found for the hybrid HTL-based devices, which makes it more compatible with roll-to-roll printing process. In the end, influence of the blend ratio of $MoO_3$ to PEDOT:PSS on photovoltaic performance and device stability was studied carefully, results indicated that the device performance would decrease with the increase of $MoO_3$ blended ratio, whereas the long-term stability was improved.

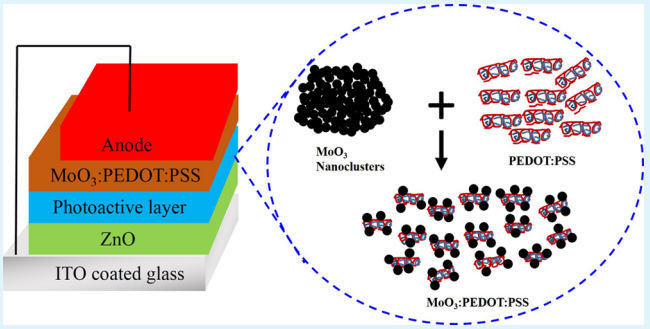


**KEYWORDS:** *inverted organic solar cell, $MoO_3$:PEDOT:PSS hybrid, hole transporting layer, improved wettability and film forming ability, thickness dependence, stability*

## 1. INTRODUCTION

The organic solar cell has the potential of fabrication through roll-to-roll (R2R) printing with the advantages of flexibility, lightweight, low cost, and ease of large-area fabrication. Impressive progress with improving power conversion efficiency of organic solar cell has been achieved in the past few years. Nowadays, high power conversion efficiencies approaching 10%[1,2] and 12%[3,4] for single junction and tandem solar cells were reported, respectively. The most widely studied organic solar cell is so-called bulk heterojunction solar cells, which consists of an organic donor−acceptor blended photoactive layer sandwiched between two electrodes.[5,6] Meanwhile, hole and electron transporting layers at the interface of organic/metal electrodes are developed to establish charge equilibrium and minimize the charge extraction barrier.[7,8]

There are two main basic structures in organic solar cells, that is, conventional and inverted structure. The inverted geometry device with a layer sequence of ITO/electron transporting layer (ETL)/photoactive layer/hole transporting layer (HTL)/metal electrode is regarded to be more ambient stable and more suitable for large-scale printing process, owing to the avoidance of using low work-function metal electrode.[9−11] In the inverted geometry device, hole transporting layer, which is characteristics with high work function and high hole mobility was proved to be essential to achieve high performance organic solar cell.[9,12,13] The most widely used

Received: December 22, 2014
Accepted: March 20, 2015
Published: March 20, 2015





DOI: 10.1021/am509049t
ACS Appl. Mater. Interfaces 2015, 7, 7170−7179

hole transporting layer in organic solar cell is poly(3,4-ethylenedioxythiohene):poly(styrenesulfonate) (PEDOT:PSS), which possesses advantages of high transparency, good conductivity, excellent mechanical flexibility and tunable work function.[7,8] However, because of the hydrophilic nature of PEDOT:PSS, it is very difficult to directly deposit PEDOT:PSS on the hydrophobic photoactive layer surface. To solve this problem, one of the methods is to add additives into PEDOT:PSS suspension to improve the wettability of PEDOT:PSS on polymer surface. For example isopropyl alcohol,[14] Triton X-100,[15] Suynole 104 series,[16] and fluorosurfactants[17−19] have been used as the additives. And the other method is surface treatment of active layer with plasma or UV-ozone to increase the surface tension.[20,21] The problem for the former method is the additives, especially the surfactants are difficult to be removed after thin film deposition, which usually impose a negative effect on device performance. For the latter one, it faces a dilemma of balance between the increasing of surface energy and possible destruction of the active layer. In addition, surface treatment is not favorable for further fabrication of tandem inverted solar cells.

An alternative to PEDOT:PSS hole transporting material is conductive metal oxide,[22] such as $MoO_3$,[12] $V_2O_5$,[9] and $WO_3$.[22−24] In particular, molybdenum oxide ($MoO_3$) is the most commonly used and most promising hole transporting material owing to its nontoxic and deep lying electronic states with high work function of 5.5−6.7 eV.[25] $MoO_3$ layers are usually deposited through thermal evaporation.[11,26] However, vacuum-related deposition process is considered as a potential drawback in term of large-area and R2R mass production. Recently, solution-processable $MoO_3$ inks have been developed, which were made from soluble Mo-based precursors, such as $Mo(CO)_3(EtCN)_3$,[27] ammonium molybdate ($(NH_4)_6Mo_7O_{24}$),[28,29] $MoO_2(acac)_2$[30−32] or from $MoO_3$ nanoparticles,[33,34] or from a so-called sol−gel method.[35,36] These $MoO_3$ inks are mostly used in conventional organic solar cells as the hole transporting layer. This is because the surface traps and relatively low charge carrier density of the solution processed metal oxide, often cause increased charge recombination and energy level misalignment at the interface of organic solar cells, and thereby reduce the device performance. For conventional organic solar cells, this problem can be simply solved by following thermal or $O_2$-plasma treatment. On the aspect of inverted solar cells, however, various following-up treatments were found to be more difficult to operate.[37−39] Another alternative method is bilayer stacked charge transporting layer or polymer:metal oxide hybrid layer.[40,41] The polymer:metal oxide hybrids show advantages of easy fabrication, good film forming ability and good device performance.[42−45] Chen et al.[22] described the use of a mixture of PEDOT:PSS and $MoO_3$ nanoparticle as hole transporting layer in conversional organic photovoltaic. In that report, the $MoO_3$ ink was prepared by hydration method, and $MoO_3$ particles with size of 10−20 nm were formed during thin film formation. Lee et al. reported the use of solution-processable vanadium oxide ($VO_x$):PSS composites for conventional organic solar cells. The work function of this $VO_x$:PSS was adjusted by changing the ratio of $VO_x$ to PSS.[46] During the revision of this article, Lee et al. reported the use of $MoO_3$:PEDOT:PSS as the HTL in inverted organic solar cell to improve the device stability.[47]

In this work, we will report the preparation, structure, and properties of $MoO_3$:PEDOT:PSS hybrid inks, which can be feasibly deposited onto the photoactive layer to form a hole transporting layer by spin coating. A core−shell structure is proposed for the first time in the $MoO_3$:PEDOT:PSS hybrid ink, where the $MoO_3$ nanoparticles connected with PSS chains act as the shell and the PEDOT chains act as the core. The devices using the $MoO_3$:PEDOT:PSS hybrid HTL present comparable power conversion efficiency as the reference thermal evaporated $MoO_3$-based devices. In addition, advantages of using this solution-processed HTL include ease of film deposition, no need for any treatment, and less HTL thickness sensitivity of device performance, which make this hybrid HTL highly compatible for R2R printing fabrication.

## 2. EXPERIMENTAL SECTION

**2.1. Materials.** Poly(3,4-ethylenedioxythiophene):poly(styrenesulfonate) (PEDOT:PSS Heraeus Clevios PVP AI 4083) was purchased from Heraeus Precious Metals GmbH & Co. KG. Regioregular poly(3-hexylthiophene) (SMI-P3HT, $M_n$ = 5.0 × $10^4$ g/mol, PDI = 1.7, regioregularity Rr = 95%) was purchased from Solarmer Energy, Inc. (Beijing). Poly[[4,8-bis[(2-ethylhexyl]oxy]-benzo[1,2-*b*:4,5-*b*′]dithiophene-2,6-diyl][3-fluoro-2-[(2-ethylhexl)-carbonyl]thieno[3,4-*b*]thiophenediyl]] (PTB7) was purchased from 1-Material. Phenyl-$C_{61}$-butyric acid methyl ester ($PC_{61}BM$) was purchased from Solenne B. V. Molybdenum powders (sized about 200 nm) were purchased from Shanghai Aladdin Reagent Co. Ltd.

**2.2. Synthesis of $MoO_3$ and $MoO_3$:PEDOT:PSS Hybrid Inks.** $MoO_3$ nanoparticles were prepared through similar route reported by Xie et al.[48] Molybdenum powder (0.25 g) was dispersed in ethanol (10 mL) under stirring for several minutes. Then $H_2O_2$ (30%, 0.5 mL) was added with continuous stirring for 24 h. After that, the reaction was terminated by stopping stirring, and followed by 1 h standing. The nanoparticles were collected through removing the solvent under vacuum. After that, the dark-blue powder was collected and redispersed in ethanol (10 mL), followed by ultrasonication for 10 min. The mixture was centrifuged at 4000 rpm for 10 min, and the solution was collected. The final $MoO_3$ nanoparticles inks were obtained by ultrasonic dispersion and finally diluted to 8 mg/mL. $MoO_3$:PEDOT:PSS hybrid inks were prepared by simply mixing the $MoO_3$ ink and PEDOT:PSS with different volume ratios.

**2.3. Material and Thin Film Characterization.** Transmission electron microscopy (TEM) and high resolution transmission electron microscopy (HRTEM) images of the $MoO_3$ nanoparticles were taken from a FEI Tecani G2 F20 S-Twin 200 kV microscope. The diameter of particles was determined by dynamic light scattering (DLS) measurements, recorded by a Malvern granulometer (Zatasizer Nano). The X-ray photoelectron spectroscopy (XPS) of the $MoO_3$ was performed on the ITO coated glass, and recorded by the Kratos Axis Ultra DLD (Kratos analytical shimadzu group company). An Al $K_\alpha$ radiation source was used for the XPS measurement.

Contact angles between the hybrid inks and the polymer surface were recorded by dynamic contact angle measuring instrument (dataphysics DCAT 21). The film thickness of the solution-processed hole transporting layer was characterized using profiler (VEECO, DEKTAK150). An average thickness error of 5 nm was taken into account since the surface was not totally homogeneous. The absorption spectra of the hole transporting layer were recorded by the Lamada 750 UV/vis/NIR spectrophotometer (PerkinElmer). The surface morphology of the films was observed by Atomic Force Microscopy (AFM), using the Agilent 550 AFM.

**2.4. Fabrication and Characterization of the Devices.** Photovoltaic devices were fabricated on indium tin oxide (ITO) coated glasses, which were cleaned by sonication in acetone, deionized water, and isopropanol, and finally $O_2$ plasma treating at 100 mW for 1 min. The 30 nm-thick ZnO layer was spin-coated from 10 mg/mL ZnO inks that dispersed in the mixture solvent of acetone and isopropanol, followed by annealing at 120 °C for 10 min in $N_2$ glovebox. For P3HT:$PC_{61}BM$-based inverted solar cells, the active layer (∼230 nm) composed of P3HT and $PC_{61}BM$ (1:1, w/w) were


DOI: 10.1021/am509049t
ACS Appl. Mater. Interfaces 2015, 7, 7170−7179

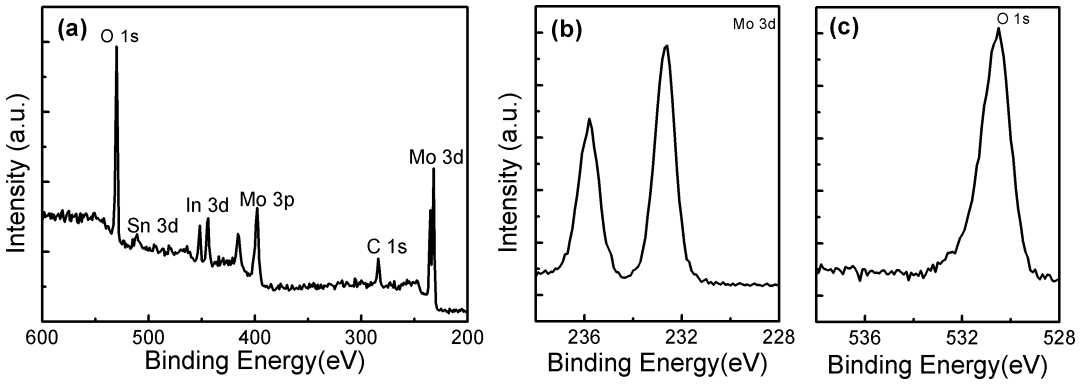


**Figure 1.** XPS spectra of the $MoO_3$ films deposited on the ITO glass. (a) Full scale, (b) Mo 3d, and (c) O 1s core level.

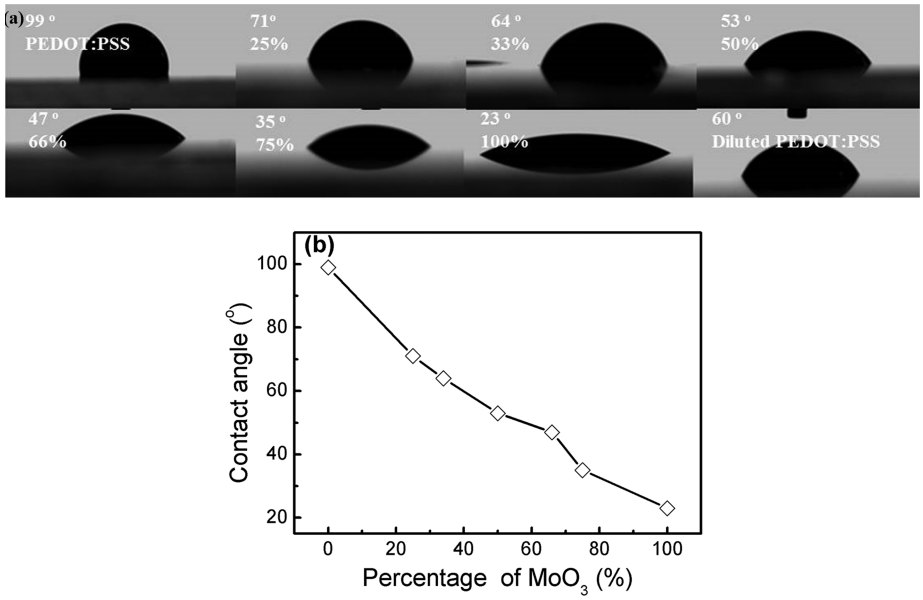


**Figure 2.** (a) Picture of a drop of PEDOT:PSS, $MoO_3$:PEDOT:PSS hybrid inks, pure $MoO_3$, and ethanol diluted PEDOT:PSS inks on the surface of P3HT:$PC_{61}$BM films. (b) The contact angle vs volume percentage of $MoO_3$ inks.

spin coated from a mixture solution of P3HT and $PC_{61}$BM in 1,2-dichlorobenzene (*o*-DCB, at a total concentration of 40 mg/mL) at 600 rpm for 120 s. Subsequently, the P3HT:$PC_{61}$BM active layers were annealed at 120 °C for 10 min in $N_2$ glovebox. On the top of the P3HT:$PC_{61}$BM active layers, $MoO_3$ or $MoO_3$:PEDOT:PSS hybrid HTLs were deposited by spin-coating from $MoO_3$ or $MoO_3$:PEDOT:PSS inks in air. Then, the films were transferred into $N_2$ glovebox and thermal treated at 120 °C for 5 min. As reference, $MoO_3$ layers (e-$MoO_3$) with different thickness were thermal evaporated above the active layer before the deposition of electrode. The thickness of e-$MoO_3$ was monitored by a quartz crystal microbalance. Finally, a 100 nm Ag or Al electrode was deposited on the HTL through thermal-evaporation at pressure about $8 \times 10^{-5}$ Pa. For the PTB7:$PC_{61}$BM-based inverted solar cell, the polymer and $PC_{61}$BM were first dissolved in chlorobenzene with ratio of 1:1.5 (PTB7:$PC_{61}$BM = 10 mg/mL:15 mg/mL) with addition of 3% volume ratio of 1,8-Diiodooctane (DIO). The 85-nm-thick active layer were spin-coated on the precoated ZnO layer and dried in vacuum chamber for 30 min. Afterward, the $MoO_3$:PEDOT:PSS hybrid hole transporting layer were spin coated in the $N_2$ glovebox. Finally, a 100 nm thick Al electrode was evaporated. The active area was 0.16 or 0.09 $cm^2$, and both devices provided similar results.

The current density–voltage (*J*–*V*) measurement was carried out under nitrogen with a Keithley 2400 source meter under simulated AM1.5 solar illumination (100 mW/$cm^2$) generated by white light from halogentungsten lamp, filtered by a Schott GG385 UV filter and a Hoya LB120 daylight filter.[49] External quantum efficiencies (EQE) were measured under simulated one sun operation conditions using bias light from a 532 nm solid state laser (Changchun New Industries, MGL-III-532). Light from a 150 W tungsten halogen lamp (Osram64610) was used as probe light and modulated with a mechanical chopper before passing the monochromator (Zolix, Omni-$\lambda$300) to select the wavelength. The response was recorded as the voltage by an *I*–*V* converter (Zolix, QE–I–V Convertor), using a lock-in amplifier (Stanford Research Systems SR 830). A calibrated Si cell was used as reference. The device was kept behind a quartz window in a nitrogen filled container. The ambient stability of devices was tested through *J*–*V* testing after storage in air for several hours without encapsulation. Samples were only illuminated during the measurements. All the measurements were carried out at room temperature.

## 3. RESULTS AND DISCUSSION

**3.1. Characterization of $MoO_3$ Nanoparticles and $MoO_3$:PEDOT:PSS Inks.** $MoO_3$ nanoparticles were synthesized by reaction of Mo powders with $H_2O_2$ in ethanol.[48] The $MoO_3$ nanoparticles inks were collected after dispersion–centrifugation-dispersion procedure. TEM and HRTEM images confirmed the formation of 5 nm-sized $MoO_3$ nanoparticles (Figure S1a and S1b in Supporting Information). HRTEM images showed lattice fringes spacing of 0.229 nm, which can


DOI: 10.1021/am509049t
ACS Appl. Mater. Interfaces 2015, 7, 7170–7179

be corresponded to the (102), (10$\bar{3}$) or (11$\bar{2}$) plane of $MoO_3$ crystals. Because these planes have very similar interplanar spaces, that is, (102) ($d$ = 0.230 nm), (10$\bar{3}$) ($d$ = 0.221 nm), or (11$\bar{2}$) ($d$ = 0.230 nm),[50] the exact indices of lattice planes could not be confirmed. X-ray photoelectron spectroscopy (XPS) spectrum was taken to confirm the valence of Mo (Figure 1). The XPS spectrum of Mo 3d core levels consist of two Gaussian-like doublets peaks cantered at 235.8 and 232.6 eV, which are contributed to the 3d orbital doublet of $Mo^{6+}$.[51,52] The O 1s peak at 530.5 eV could be attributed to the $O^{2-}$ in $MoO_3$.[51,53] The XPS spectrum excluded the existence of other impurities. With these, one can conclude that the synthesized nano-$MoO_3$ were crystalline $MoO_3$ nanoparticles. The synthesized $MoO_3$ nanoparticles can be easily dispersed in ethanol, and $MoO_3$ ink (8 mg/mL) was prepared by dispersing the $MoO_3$ nanoparticle in ethanol. The $MoO_3$ ink is blue in color (Supporting Information Figure S1d) and stable enough to be kept in ambient condition for 3 months without obvious precipitation or change in color.

The $MoO_3$:PEDOT:PSS hybrid inks were prepared by simply mixing the $MoO_3$-ethanol ink and PEDOT:PSS (VP AI4083) aqueous solution together in a proper volume ratio. The $MoO_3$:PEDOT:PSS hybrid inks are also blue in color (Supporting Information Figure S1d). HRTEM images of the PEDOT:PSS:$MoO_3$ hybrid film formed by dropping the hybrid ink onto the copper mesh also showed the lattice fringes of $MoO_3$ (Supporting Information Figure S1c). Furthermore, EDX analysis on the $MoO_3$ and $MoO_3$:PEDOT:PSS films on the P3HT:$PC_{61}$BM surface confirmed the existence of Mo element (Table S1 and S2 in Supporting Information). Together with atomic force microscopy images (AFM) and dynamic light scattering (DLS) analysis results (vide infra), one can conclude that $MoO_3$ nanoparticles are well intermixed with PEDOT:PSS. No precipitate was found for the fresh prepared $MoO_3$:PEDOT:PSS hybrid inks regardless to the content ratio of $MoO_3$ to PEDOT:PSS in the first some hours, which makes the fresh-prepared $MoO_3$:PEDOT:PSS hybrid inks suitable for further device fabrication.

Figure 2a shows the contact angles between the $MoO_3$:PEDOT:PSS ink and P3HT:$PC_{61}$BM surface. As can be seen from this figure, the contact angle of PEDOT:PSS (AI 4083) on polymer surface is around 99°, suggesting a nonwettable property between the pristine PEDOT:PSS ink and P3HT:$PC_{61}$BM surface. On the other hand, the $MoO_3$ ink shows a good wettability on the polymer surface with a contact angle of 23°. With the increase of the content of $MoO_3$ in the mixture, the contact angle decreases gradually from 99° to 23° (Figure 2b), suggesting an improved wettability between the $MoO_3$:PEDOT:PSS ink and the polymer surface, which provides the possibility of depositing $MoO_3$:PEDOT:PSS layer on the top of P3HT:$PC_{61}$BM layer directly.

Figure 3 depicts the atomic force microscopy (AFM) morphology images of P3HT:$PC_{61}$BM surface coated with $MoO_3$ or $MoO_3$:PEDOT:PSS (50%:50% v/v). As can be seen from Figure 3a, the P3HT:$PC_{61}$BM/$MoO_3$ surface was quite rough with a root-mean-square roughness (RMS) of 2.8 nm. Particles with large size distributions (30−200 nm) were found on the surface, which could be attributed to the agglomeration of $MoO_3$ nanoparticles during the thin film deposition. Similar results were found in other metal oxide film, such as ZnO films.[54] The aggregation of $MoO_3$ nanoparticles were greatly suppressed in $MoO_3$:PEDOT:PSS hybrid thin film. As can be seen from Figure 3b, small isolated particles with size around 5

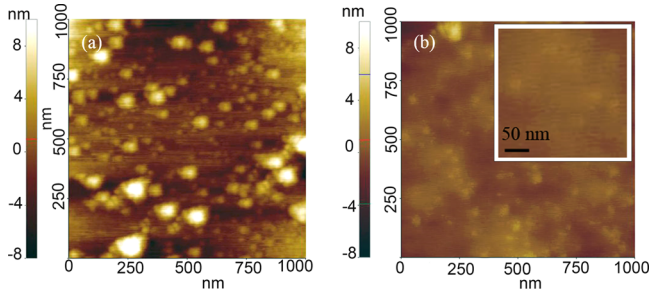


**Figure 3.** AFM topographic images of the (a) P3HT:$PC_{61}$BM (230 nm)/$MoO_3$ (60 nm) and (b) P3HT:$PC_{61}$BM (230 nm)/$MoO_3$:PEDOT:PSS (50%:50% v/v, 50 nm) films.

nm are distributed more homogeneously over the surface (Figure 3b, insert). Such small particles were then ascribed to the $MoO_3$ nanocrystals. This unambiguously confirmed that $MoO_3$ nanoparticles were intermixed with PEDOT:PSS and both $MoO_3$ and PEDOT:PSS were deposited onto polymer surface. In addition, a smoother surface (RMS = 0.8 nm) of P3HT:$PC_{61}$BM/$MoO_3$:PEDOT:PSS (50%:50% v/v) was found, suggesting that the use of polymeric polyelectrolyte together with metal oxide nanoparticles could smooth the surface. This phenomenon was also found in ZnO-PVP hybrid.[42] The deposition of $MoO_3$ and $MoO_3$:PEDOT:PSS layers on P3HT:$PC_{61}$BM surface was further confirmed by the UV−vis absorption spectroscopy. Compared to the P3HT:$PC_{61}$BM pristine film, enhanced absorption intensity over 250−300 and 700−800 nm was found after deposition of $MoO_3$ or $MoO_3$:PEDOT:PSS layer (Figure S2 in Supporting Information), which was attributed the absorption of $MoO_3$ and PEDOT:PSS.[55,56] Overall, it is clear that $MoO_3$:PEDOT:PSS can be easily deposited on hydrophobic polymer surface to form a more uniform and homogeneous surface without any surface treatment, which makes $MoO_3$:PEDOT:PSS a good HTL for use in inverted organic solar cells.

It is worth to note that the contact angle of ethanol diluted PEDOT:PSS (50%:50% v/v) on P3HT:$PC_{61}$BM surface was about 60°, which was similar to that of $MoO_3$:PEDOT:PSS (50%:50% v/v) (53°). Since the $MoO_3$ ink is dispersed in ethanol, this result suggests that the improved wettability of $MoO_3$:PEDOT:PSS hybrid inks could be due to the addition of ethanol. However, the UV−vis absorption spectrum of P3HT:$PC_{61}$BM film after being spin-coated an ethanol diluted PEDOT:PSS solution was found to be identical to that of the pristine polymer film (Supporting Information Figure S2c). This indicated that no PEDOT:PSS film was deposited onto the P3HT:$PC_{61}$BM surface from the diluted PEDOT:PSS solution. Optical microscope images comparison also supported this conclusion (Supporting Information Figure S3). This means, although the addition of ethanol to PEDOT:PSS solution could improve the wettability of the ink, the adhesion of PEDOT:PSS on the underlying hydrophobic polymeric layer was not good enough to form a defined HTL. It is therefore reasonable to ascribe the improvement of film forming properties to the addition of $MoO_3$ nanoparticles ink rather than simple solvent effect.

It is known that PEDOT:PSS is composed of hydrophobic PEDOT and hydrophilic PSSH chains, which are attached together through Coulombic attraction in a necklace structure with the PEDOT as the core and PSS as the shell,


DOI: 10.1021/am509049t
ACS Appl. Mater. Interfaces 2015, 7, 7170−7179

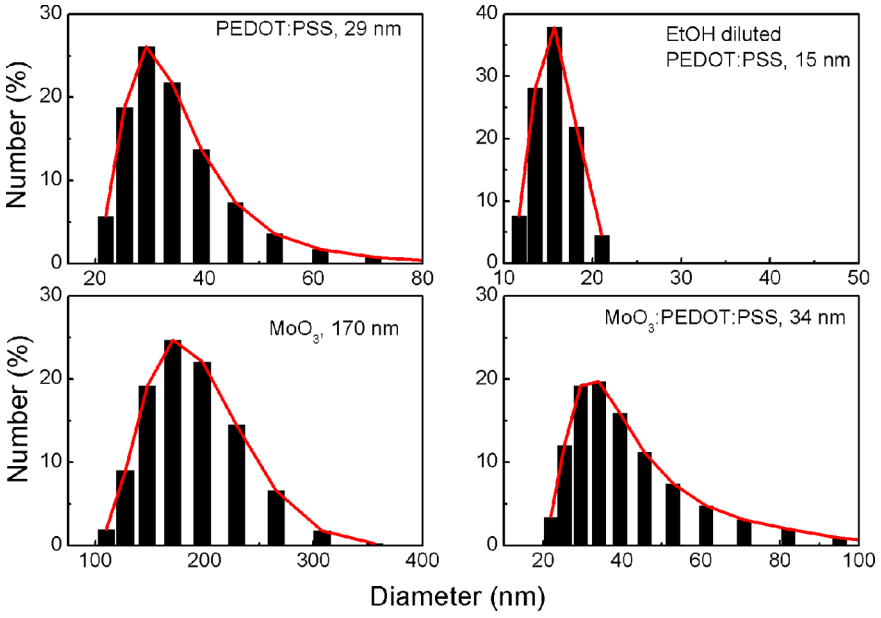


**Figure 4.** Particle diameter of PEDOT:PSS, ethanol diluted PEDOT:PSS ink, $MoO_3$ nanoparticles inks, and $MoO_3$:PEDOT:PSS hybrid ink, recorded by dynamic light scattering (DLS) measurement.

respectively.[57] From dynamic light scattering measurement (DLS), it was found that PEDOT:PSS formed colloids sizing around 29 nm in aqueous solution (Figure 4), which was similar to the result reported in the literature.[58] The ethanol diluted PEDOT:PSS shows a decreased diameter about 15 nm, which may due to reduced aggregation effect. On the other hand, DLS measurement showed that $MoO_3$ nanoparticles formed large clusters in ethanol with sizes around 100−200 nm (Figure 4). The measured cluster size of $MoO_3$ by DSL is corresponding reasonable well with that measured by AFM (Figure 3a). Upon the addition of PEDOT:PSS into $MoO_3$, however, large $MoO_3$ nanocluster was not detected any more, and small particles with average diameters around 34 nm were found in the hybrid solution (Figure 4). The measured average $MoO_3$:PEDOT:PSS colloid size (~34 nm) was nearly the sum of four $MoO_3$ nanoparticle and the average size of PEDOT:PSS colloid that diluted in ethanol, suggesting that $MoO_3$ particle is attached on the PEDOT:PSS colloid in an average number ratio as 4:1. Efforts to understand the $MoO_3$:PEDOT:PSS nanostructure with TEM technology have been made, however, no successful result was achieved yet, which was due to the high contents of light elements (such as, C, O, S) in PEDOT:PSS. Nevertheless, taking it into account that PEDOT:PSS has a core−shell structure in aqueous and hydrophilic $MoO_3$ is preferentially connected with hydrophilic PSS chain, a core−shell structured $MoO_3$:PEDOT:PSS composite with hydrophobic PEDOT as the core and PSS-$MoO_3$ as the shell in the hybrid ink was proposed (Figure 5).

On the basis of the experimental results, the mechanism for the improvement in film forming ability for $MoO_3$:PEDOT:PSS might be originated from two aspects, that is, effect of ethanol solvent and effect of $MoO_3$ nanoparticles: First, the wettability of PEDOT:PSS on the polymer surface was improved through the addition of ethanol which caused significant decrease of surface energy. Second, the addition of $MoO_3$ nanoparticles increased the adhesion between HTL layer and photoactive layer, and thus helped to form a smooth $MoO_3$:PEDOT:PSS film.

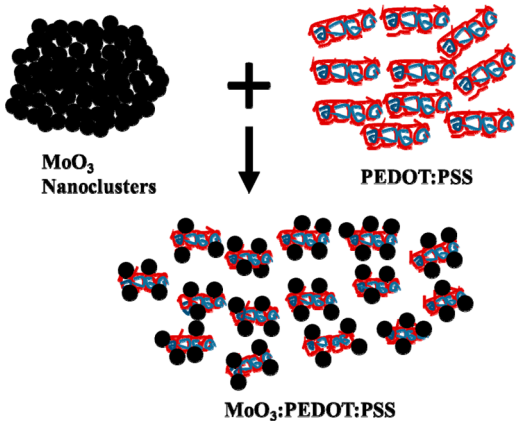


**Figure 5.** Schematic depiction of the structure of PEDOT:PSS and $MoO_3$:PEDOT:PSS. The blue line, red line, and the black dot represent the PEDOT, PSS chain, and the $MoO_3$ nanoparticles, respectively.

### 3.2. Characterization of the Inverted Solar Cells.

*3.2.1. HTL Thickness Dependence.* Inverted polymer solar cells with the structure of ITO/ZnO/P3HT:$PC_{61}BM$/HTL/Ag or Al were fabricated, where the hole transporting layer (HTL) was deposited either by vacuum evaporation of $MoO_3$ powder or solution-based spin-coating from $MoO_3$, or $MoO_3$:PEDOT:PSS (50%:50% v/v) hybrid inks. As reference, devices without HTL were also fabricated and tested. Tables 1 and 2 list the best device performance data for solar cells using Ag and Al counter electrode, respectively. And Figure 6 shows the *J*−*V* curves of the highest performance cells. Statistical analyses on 8 individual devices for each type of solar cell were also performed, and the full versions of results are listed in Supporting Information (Tables S3 and S4). For better comparison, the averaged power conversion efficiencies including standard deviations are also listed in Tables 1 and 2 accordingly. As can be seen from these tables, these average performance values showed similar variation tendency as to that of the best device on the thickness dependence. As shown in


DOI: 10.1021/am509049t
ACS Appl. Mater. Interfaces 2015, 7, 7170−7179

**Table 1. Photovoltaic Performance Parameters of the Best P3HT:$PC_{61}BM$ Solar Cells with Ag Electrode**

| entry | device | thickness (nm) | $V_{OC}$ (V) | $J_{SC}$ (mA/cm$^2$) | FF (%) | PCE (%) | av PCE ± std. dev. (%)[a] |
|---|---|---|---|---|---|---|---|
| 1 | w/o | 0 | 0.28 | 5.33 | 36 | 0.54 | |
| 2 | e-$MoO_3$ | 5 | 0.58 | 6.79 | 64 | 2.52 | 2.49 ± 0.05 |
| 3 | e-$MoO_3$ | 10 | 0.56 | 8.04 | 63 | 2.84 | 2.77 ± 0.05 |
| 4 | e-$MoO_3$ | 20 | 0.60 | 7.64 | 66 | 3.03 | 2.84 ± 0.04 |
| 5 | e-$MoO_3$ | 30 | 0.61 | 6.95 | 66 | 2.80 | 2.73 ± 0.04 |
| 6 | e-$MoO_3$ | 50 | 0.60 | 6.60 | 58 | 2.30 | 2.22 ± 0.11 |
| 7 | s-$MoO_3$ | 60 | 0.60 | 6.42 | 58 | 2.23 | 2.02 ± 0.12 |
| 8 | $MoO_3$:PEDOT:PSS | 30 | 0.61 | 7.71 | 62 | 2.92 | 2.87 ± 0.06 |
| 9 | $MoO_3$:PEDOT:PSS | 50 | 0.61 | 7.85 | 61 | 2.92 | 2.86 ± 0.05 |
| 10 | $MoO_3$:PEDOT:PSS | 75 | 0.60 | 7.51 | 63 | 2.84 | 2.78 ± 0.09 |

[a]Statistical parameters are calculated over 8 individual devices.

**Table 2. Photovoltaic Performance Parameters of the Best P3HT:$PC_{61}BM$ Solar Cells with Al Electrode**

| entry | device | thickness (nm) | $V_{OC}$ (V) | $J_{SC}$ (mA/cm$^2$) | FF (%) | PCE (%) | av PCE ± std. dev. (%)[a] |
|---|---|---|---|---|---|---|---|
| 11 | e-$MoO_3$ | 20 | 0.60 | 7.94 | 64 | 3.05 | 2.97 ± 0.24 |
| 12 | $MoO_3$:PEDOT:PSS | 30 | 0.61 | 8.57 | 63 | 3.29 | 3.10 ± 0.07 |
| 13 | $MoO_3$:PEDOT:PSS | 50 | 0.61 | 8.18 | 61 | 3.04 | 2.97 ± 0.07 |
| 14 | $MoO_3$:PEDOT:PSS | 75 | 0.61 | 7.86 | 62 | 2.97 | 2.71 ± 0.17 |

[a]Statistical parameters are calculated over 8 individual devices.

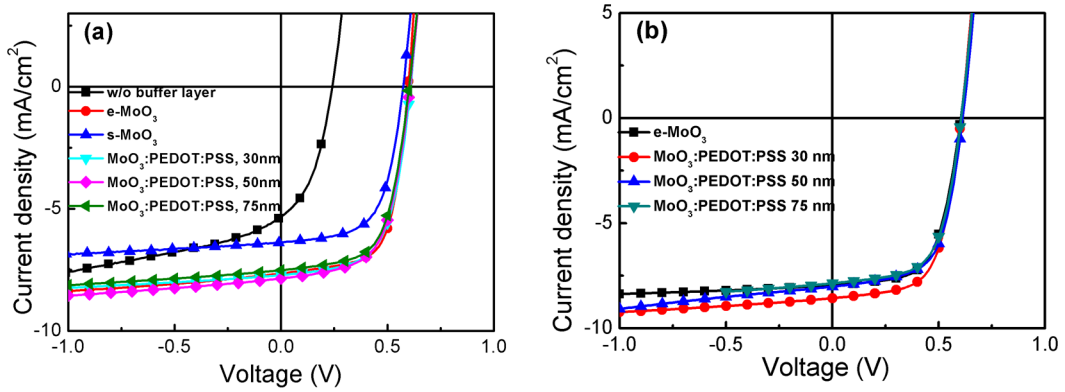


**Figure 6.** $J-V$ characteristics of the inverted solar cells with e-$MoO_3$, solution-processed $MoO_3$, and $MoO_3$:PEDOT:PSS hybrid HTL for (a) Ag and (b) Al electrodes involved devices.

Table 1, the device without HTL showed very poor characteristics with a $V_{OC}$ of 0.28 V, $J_{SC}$ of 5.33 mA/cm$^2$, FF of 36%, and PCE of 0.54%. Device performance was greatly improved by insertion of a thin HTL layer. For example, device with 5 nm vacuum deposited $MoO_3$ layer showed a $V_{OC}$ of 0.58 V, $J_{SC}$ of 6.79 mA/cm$^2$, FF of 64%, and PCE of 2.52%. The highest device performance was achieved with 20 nm e-$MoO_3$, which showed a power conversion efficiency of 3.03%. The increase of $V_{OC}$ and FF could be attributed to a better energy level alignments between the photoactive layer and back electrode.[59,60] Meanwhile, the increase of $J_{SC}$ might be originated from the enhanced light harvesting because of optical spacer effect.[61] Compared with device using e-$MoO_3$ hole transporting layer, solution-processed $MoO_3$ HTL (entry 6, HTL layer thickness of 60 nm) involved devices displayed similar $V_{OC}$ but lower $J_{SC}$ and FF. This might be due to the poor coverage and high roughness of solution-processed $MoO_3$ film, supported by the atomic force microscopy (AFM) images of the P3HT:$PC_{61}BM$/$MoO_3$ film (Figure 3a).

In contrast, the $MoO_3$:PEDOT:PSS layer-based devices showed similar device performance to that of device using 20 nm e-$MoO_3$ HTL. All these $MoO_3$:PEDOT:PSS based devices showed $V_{OC}$ around 0.61 V and high FF of more than 61%, whereas $J_{SC}$ varied slightly with different HTL layer thickness. For devices with Al electrode (Figure 6b and Table 2), the device performance was improved slightly when compared with that using Ag as the back electrode. The device with 30 nm-thick $MoO_3$:PEDOT:PSS HTL gave a best PCE of 3.29%, with $V_{OC}$ of 0.61 V, $J_{SC}$ of 8.57 mA/cm$^2$, and FF of 63%, which was also comparable with the optimized control device using a 20 nm thick thermally evaporated $MoO_3$ HTL.

It is worth noting that device with e-$MoO_3$ as the HTL was found to be highly depended on the HTL-thickness (Table 1 and Supporting Information Figure S4). When the thickness of e-$MoO_3$ was higher than 30 nm, device performance started to decrease. While devices using $MoO_3$:PEDOT:PSS as the HTL showed much less HTL layer thickness dependence. All these device showed similar $V_{OC}$ around 0.61 V and high FF (>61%), whereas the variation of $J_{SC}$ was mainly attributed the optical spacer effect,[61] which suggested that a low thickness depended hole transporting property of the $MoO_3$:PEDOT:PSS layer. In addition, the $MoO_3$:PEDOT:PSS hybrid HTL was deposited onto the organic photoactive layer without the need of any further surface treatment like UV ozone, plasma or adding


DOI: 10.1021/am509049t
ACS Appl. Mater. Interfaces 2015, 7, 7170−7179

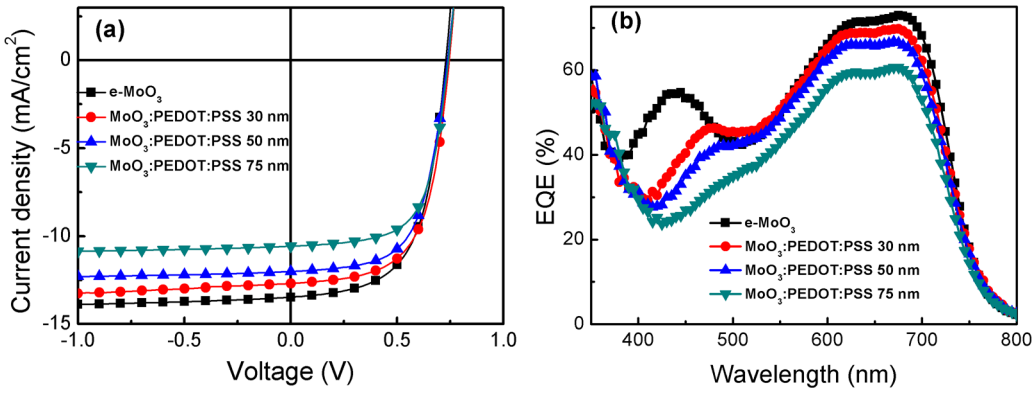


**Figure 7.** (a) $J-V$ characteristics of the PTB7:$PC_{61}BM$ inverted solar cells. (b) EQE spectra of the PTB7:$PC_{61}BM$ inverted solar cells.

**Table 3. Performance Parameters of the PTB7:$PC_{61}BM$ Solar Cells with Al Electrode**

| entry | device | thickness (nm) | $V_{OC}$ (V) | $J_{SC}$ (mA/cm$^2$) | FF (%) | PCE (%) | av PCE ± std. dev. (%)[a] |
|---|---|---|---|---|---|---|---|
| 15 | e-$MoO_3$ | 20 | 0.73 | 13.5 | 61 | 6.01 | 5.56 ± 0.40 |
| 16 | $MoO_3$:PEDOT:PSS | 30 | 0.74 | 12.7 | 63 | 5.92 | 5.76 ± 0.17 |
| 17 | $MoO_3$:PEDOT:PSS | 50 | 0.74 | 12.0 | 63 | 5.59 | 5.36 ± 0.27 |
| 18 | $MoO_3$:PEDOT:PSS | 75 | 0.74 | 10.7 | 65 | 5.15 | 5.04 ± 0.04 |

[a]Statistical parameters are calculated over 8 individual devices.

**Table 4. Solar Cell Parameters of the P3HT:$PC_{61}BM$-Based Inverted Solar Cells, Using Hybrid HTL with Different Content of $MoO_3$[a]**

| entry | $MoO_3$:PEDOT:PSS ratio (v/v) | $V_{OC}$ (V) | $J_{SC}$ (mA/cm$^2$) | FF (%) | PCE (%) | av PCE ± std. dev. (%)[a] |
|---|---|---|---|---|---|---|
| 19 | 25%:75% | 0.61 | 8.85 | 61 | 3.29 | 3.25 ± 0.06 |
| 20 | 33%:67% | 0.61 | 8.89 | 57 | 3.09 | 3.00 ± 0.10 |
| 21 | 50%:50% | 0.61 | 8.88 | 60 | 3.25 | 3.11 ± 0.13 |
| 22 | 66%:34% | 0.60 | 8.27 | 60 | 2.98 | 2.85 ± 0.19 |
| 23 | 75%:25% | 0.60 | 8.23 | 60 | 2.96 | 2.89 ± 0.17 |
| 24 | 80%:20% | 0.58 | 8.11 | 58 | 2.73 | 2.52 ± 0.19 |
| 25 | 90%:10% | 0.57 | 7.01 | 53 | 2.12 | 2.02 ± 0.27 |
| 26 | 100%:0% | 0.58 | 6.84 | 56 | 2.23 | 2.00 ± 0.25 |

[a]Statistical parameters are calculated over 8 individual devices.

other surfactants. These characteristic advantages make it compatible for R2R printing processing, for which the larger thickness toleration is a prerequisite for the high reproducibility.

Additionally, the PTB7:$PC_{61}BM$ inverted solar cells were also fabricated. As shown from the $J-V$ characteristics (Figure 7a) and device performance (Table 3, see Supporting Information Table S5 for full version of device performance), the control device using evaporated $MoO_3$ HTL gave the performance of $V_{OC}$ = 0.73 V, $J_{SC}$ = 13.50 mA/cm$^2$, FF = 61%, and PCE = 6.01%. And for hybrid HTL involved inverted solar cell, the device with 30 nm-thick $MoO_3$:PEDOT:PSS gave the best PCE of 5.92%, with $V_{OC}$ of 0.74 V, $J_{SC}$ of 12.7 mA/cm$^2$, and FF of 63%. For the hybrid HTL device, the $J_{SC}$ decreased with the increase of HTL thickness, while the $V_{OC}$ and FF seemed to be thickness-independent. The EQE spectra (Figure 7b) showed that the thicker of HTL, the lower EQE, which was in consistent with the variation of $J_{SC}$. Note that FF was as high as 65% when the $MoO_3$:PEDOT:PSS was 75 nm thick, suggesting a good hole transporting and injection ability of this layer. The decrease of $J_{SC}$ was then mainly ascribed to the optical spacer effect.[61] It implied that the thickness of photoactive layer and HTL is needed to be collaborative optimized to gain higher performance for PTB7:$PC_{61}BM$ device.

*3.2.2. Effect of Blending Ratio on Device Performance and Stability.* For real application of this $MoO_3$:PEDOT:PSS hybrid ink, stability is one of the key issue needed to be clarified. To understand the influence of blend ratio of $MoO_3$ to PEDOT:PSS on ink stability, a series of $MoO_3$:PEDOT:PSS hybrid inks with different blended volume ratios were prepared. Supporting Information Figure S5 shows the photographs of these hybrid inks after aging for different times. As can be seen clearly here, the hybrid inks with 25%, 33%, or $x$% ($x$ > 75) $MoO_3$ were stable after stored in ambient for 8 days, whereas precipitates were found in the hybrid inks with 50%, 66%, and 75% $MoO_3$. The reason for the stability difference of the hybrid inks was proposed to be the different surface charge density of the $MoO_3$:PEDOT:PSS colloids in the different blend ratios, which would lead to balanced or unbalanced surface charge in different mixture solvents. However, more experiments are still needed to fully understand the mechanism. Nevertheless, such an experiment provided important stability information on the hybrid inks.

In the next step, a series of inverted solar cells using those HTLs were fabricated to understand the influence of $MoO_3$ content on the device performance. Table 4 lists the photovoltaic performances of device with different HTLs. As can be seen from this table, device performance is indeed


DOI: 10.1021/am509049t
ACS Appl. Mater. Interfaces 2015, 7, 7170−7179

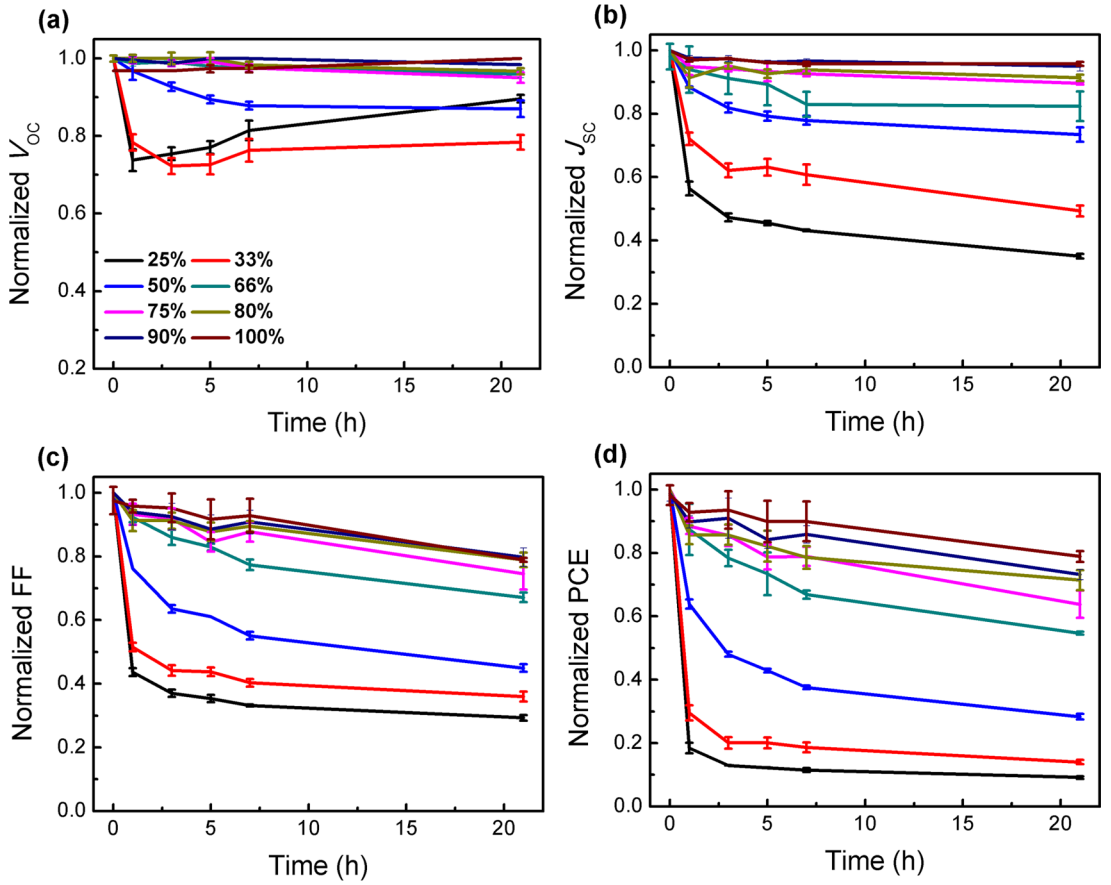


**Figure 8.** Normalized (a) $V_{OC}$, (b) $J_{SC}$, (c) FF, and (d) PCE values as a function of exposure time in ambient for P3HT:$PC_{61}BM$ solar cells with different hybrid hole transporting layers. The statistical deviation is calculated over 4 individual devices.

depended on the $MoO_3$ content. When the $MoO_3$ content is less than 50%, high performance of around 3% was able to achieved, whereas when the $MoO_3$:PEDOT:PSS blended ratio is higher than 50%, $J_{SC}$ decreased rapidly with the increase of $MoO_3$ content. The reason for $MoO_3$ content relied device performance was ascribed to the unfavorable surface morphology of HTL with more $MoO_3$ (vide supra).

In addition, the long-term stability of devices was also found to be the blend ratio related. Figure 8 depicts the evolution of $V_{OC}$, $J_{SC}$, FF, and PCE of unencapsulated P3HT:$PC_{61}BM$ inverted solar cells with different HTLs after storage in the air. As can be seen from this figure, the stability was improved with the increase of $MoO_3$ content of the HTL layer. The higher PEDOT:PSS content lead to a faster degradation, indicating that the hygroscopic of PEDOT:PSS was the main reason for the device degradation.[62] Interestingly, for $V_{OC}$, only slight variation was observed for devices with hybrid HTL that containing higher content of $MoO_3$ (≥66%). While the $V_{OC}$ for devices with $MoO_3$:PEDOT:PSS bend ratio of 25% (entry 19), 33% (entry 20), and 50% (entry 21) declined very fast at the first some hours, and then turned to be rather stable (entry 21) or even increased slightly (entry 19 and 20). The reason for the increase of $V_{OC}$ is not clear yet. However, the low $J_{SC}$ and FF of this device and a typical "S-shape" $J$–$V$ curve of the device (Supporting Information Figure S6) suggests the formation of interface diploe moment after aging.[63] In contrast to $V_{OC}$, the decrease of $J_{SC}$ and FF was found to be more significant than that of $V_{OC}$, demonstrating that the degradation might be more related with the interface changes. As shown in Supporting Information Figure S7, for entry 19, where the blend ratio of $MoO_3$ to PEDOT:PSS is 25%:75%, the $R_s$ increased from 6 to 335 Ω·$cm^2$ (56 times), and the $R_{sh}$ decreased from 686 to 146 Ω·$cm^2$ (1/4), whereas for entry 25, where the blend ratio of $MoO_3$ to PEDOT:PSS is 90%:10%, the $R_s$ increased only slightly from 6 to 30 Ω$cm^2$ (5 times), while the $R_{sh}$ decreased from 988 to 660 Ω $cm^2$ (2/3). Such series and shunt resistance changes were then ascribed to the interface changes. Overall, it could be concluded that the HTL-organic and HTL-metal electrode interfaces are more stable with high $MoO_3$ content, which improve the device stability.

## 4. CONCLUSIONS

In summary, we have shown in this manuscript a solution-processed $MoO_3$:PEDOT:PSS hybrid layer for use in inverted organic solar cells as the hole transporting layer. By mixing PEDOT:PSS with $MoO_3$ nanocrystals, the preferential connection of $MoO_3$ with PSS lead to the formation of a composite core–shell structure with PEDOT as the core and $MoO_3$:PSS as the shell, respectively. Such a hybrid ink has improved wettability and film forming ability on the polymer surface. Because of strong adhesion of $MoO_3$ with photoactive layer, uniform and smooth $MoO_3$:PEDOT:PSS hybrid films can be easily deposited on the top of photoactive layers without any surface treatment. In addition, since the $MoO_3$ nanoparticles attached to PSS-shell, aggregation of $MoO_3$ nanoparticles was greatly suppressed when compared to the bare $MoO_3$ nanoparticles ink, which yields smooth surface. P3HT:$PC_{61}BM$- and PTB7:$PC_{61}BM$-based solar cells using


DOI: 10.1021/am509049t
ACS Appl. Mater. Interfaces 2015, 7, 7170–7179

the $MoO_3$:PEDOT:PSS hybrid layer showed comparable performance as the e-$MoO_3$ HTL employed reference devices. In addition, the $MoO_3$:PEDOT:PSS hybrid HTL based devices showed low layer thickness dependence, which is a great application potential for roll-to-roll printing processing. Finally, the influence of the blend ratio of $MoO_3$ and PEDOT:PSS on device performance and device stability was also investigated. Results indicated that device with high content of $MoO_3$ presented lower device performance because of the poor film surface morphology but improved device long-term stability because of the more stable interface.

## ■ ASSOCIATED CONTENT

### Supporting Information

TEM, HRTEM, and EDX analysis results, photograph of the $MoO_3$ and $MoO_3$:PEDOT:PSS hybrid inks after aging, absorption spectra of various films, and full version of statistical photovoltaic performance data. This material is available free of charge via the Internet at http://pubs.acs.org.

## ■ AUTHOR INFORMATION


### Corresponding Authors

*E-mail: qluo2011@sinano.ac.cn.
*E-mail: cqma2011@sinano.ac.cn.


### Notes

The authors declare no competing financial interest.

## ■ ACKNOWLEDGMENTS

The work is financially supported by the National Natural Science Foundation of China (61306073, 91123034),Strategic Priority Research Program of the Chinese Academy of Sciences (Grant No. XDA09020201), and Jiangshu Provincial Natural Science Foundation (BK20130346).

## ■ REFERENCES


(1) Ye, L.; Zhang, S.; Zhao, W.; Yao, H.; Hou, J. Highly Efficient 2D-Conjugated Benzodithiophene-Based Photovoltaic Polymer with Linear Alkylthio Side Chain. *Chem. Mater.* **2014**, *26*, 3603−3605.

(2) He, Z. C.; Zhong, C. M.; Su, S. J.; Xu, M.; Wu, H. B.; Cao, Y. Enhanced Power-Conversion Efficiency in Polymer Solar Cells Using an Inverted Device Structure. *Nat. Photonics* **2012**, *6*, 591−595.

(3) You, J. B.; Dou, L. T.; Yoshimura, K.; Kato, T.; Ohya, K.; Moriarty, T.; Emery, K.; Chen, C. C.; Gao, J.; Li, G.; Yang, Y. A Polymer Tandem Solar Cell with 10.6% Power Conversion Efficiency. *Nat. Commun.* **2013**, *4*, 1446.

(4) Chen, C.-C.; Chang, W.-H.; Yoshimura, K.; Ohya, K.; You, J.; Gao, J.; Hong, Z.; Yang, Y. An Efficient Triple-Junction Polymer Solar Cell Having a Power Conversion Efficiency Exceeding 11%. *Adv. Mater.* **2014**, *26*, 5670−5677.

(5) Brabec, C. J.; Sariciftci, N. S.; Hummelen, J. C. Plastic Solar Cells. *Adv. Funct. Mater.* **2001**, *11*, 15−26.

(6) Blom, P. W. M.; Mihailetchi, V. D.; Koster, L. J. A; Markov, D. E. Device Physics of Polymer: Fullerene Bulk Heterojunction Solar Cells. *Adv. Mater.* **2007**, *19*, 1551−1566.

(7) Ma, H.; Yip, H. L.; Huang, F.; Jen, A. K. Y. Interface Engineering for Organic Electronics. *Adv. Funct. Mater.* **2010**, *20*, 1371−1388.

(8) Po, R.; Carbonera, C.; Bernardi, A.; Camaioni, N. The Role of Buffer Layers in Polymer Solar Cells. *Energy Environ. Sci.* **2011**, *4*, 285−310.

(9) Zilberberg, K.; Trost, S.; Meyer, J.; Kahn, A.; Behrendt, A.; Lutzenkirchen-Hecht, D.; Frahm, R.; Riedl, T. Inverted Organic Solar Cells with Sol−Gel Processed High Work-Function Vanadium Oxide Hole-Extraction Layers. *Adv. Funct. Mater.* **2011**, *21*, 4776−4783.

(10) Hau, S. K.; Yip, H. L.; Baek, N. S.; Zou, J. Y.; O'Malley, K.; Jen, A. K. Y. Air-Stable Flexible Polymer Solar Cells Using Zinc Oxide Nanoparticles as an Electron Selective Layers. *Appl. Phys. Lett.* **2008**, *92*, No. 253301.

(11) Zhang, F. J.; Xu, X. W.; Tang, W. H.; Zhang, J.; Zhuo, Z. L.; Wang, J.; Wang, J.; Xu, Z.; Wang, Y. S. Recent Development of the Inverted Configuration Organic Solar Cells. *Sol. Energy Mater. Sol. Cells* **2011**, *95*, 1785−1799.

(12) Li, G.; Chu, C. W.; Shrotriya, V.; Huang, J.; Yang, Y. Efficient Inverted Polymer Solar Cells. *Appl. Phys. Lett.* **2006**, *88*, No. 073508.

(13) Hau, S. K.; Yip, H. L.; Jen, A. K. Y. A Review on the Development of the Inverted Polymer Solar Cell Architecture. *Polym. Rev.* **2010**, *50*, 474−510.

(14) Stubhan, T.; Ameri, T.; Salinas, M.; Krantz, J.; Machui, F.; Halik, M.; Brabec, C. J. High Shunt Resistance in Polymer Solar Cells Comprising a $MoO_3$ Hole Extraction Layer Processed from Nanoparticle Suspension. *Appl. Phys. Lett.* **2011**, *98*, No. 253308.

(15) Baek, W. H.; Choi, M.; Yoon, T. S.; Lee, H. H.; Kim, Y. S. Use of Fluorine-Doped Tin Oxide Instead of Indium Tin Oxide in Highly Efficient Air-Fabricated Inverted Polymer Solar Cells. *Appl. Phys. Lett.* **2010**, *96*, No. 133506.

(16) Heo, S. W.; Baek, K. H.; Lee, T. H.; Lee, J. Y.; Moon, D. K. Enhanced Performance in Inverted Polymer Solar Cells Via Solution Process: Morphology Controlling of PEDOT:PSS as Anode Buffer Layer by Adding Surfactants. *Org. Electron.* **2013**, *14*, 1629−1635.

(17) Lim, F. J.; Ananthanarayanan, K.; Luther, J.; Ho, G. W. Influence of a Novel Fluorosurfactant Modified PEDOT:PSS Hole Transport Layer on the Performance of Inverted Organic Solar Cells. *J. Mater. Chem.* **2012**, *22*, 25057−25064.

(18) Chen, Y. L.; Kao, W. S.; Tsai, C. E.; Lai, Y. Y.; Cheng, Y. J.; Hsu, C. S. A New Ladder-Type Benzodi(Cyclopentadithiophene)-Based Donor-Acceptor Polymer and a Modified Hole-Collecting PEDOT:PSS Layer to Achieve Tandem Solar Cells with an Open-Circuit Voltage of 1.62 V. *Chem. Commun.* **2013**, *49*, 7702−7704.

(19) Lipomi, D. J.; Tee, B. C. K.; Vosgueritchian, M.; Bao, Z. N. Stretchable Organic Solar Cells. *Adv. Mater.* **2011**, *23*, 1771−1775.

(20) Voigt, M. M.; Mackenzie, R. C. I.; Yau, C. P.; Atienzar, P.; Dane, J.; Keivanidis, P. E.; Bradley, D. D. C.; Nelson, J. Gravure Printing for Three Subsequent Solar Cell Layers of Inverted Structures on Flexible Substrates. *Sol. Energy Mater. Sol. Cells* **2011**, *95*, 731−734.

(21) Kouijzer, S.; Esiner, S.; Frijters, C. H.; Turbiez, M.; Wienk, M. M.; Janssen, R. A. J. Efficient Inverted Tandem Polymer Solar Cells with a Solution-Processed Recombination Layer. *Adv. Energy Mater.* **2012**, *2*, 945−949.

(22) Chen, L.; Wang, P.; Li, F.; Yu, S.; Chen, Y. Efficient Bulk Heterojunction Polymer Solar Cells Using PEDOT/PSS-Doped with Solution-Processed $MoO_3$ as Anode Buffer Layer. *Sol. Energy Mater. Sol. Cells* **2012**, *102*, 66−70.

(23) Stubhan, T.; Li, N.; Luechinger, N. A.; Halim, S. C.; Matt, G. J.; Brabec, C. J. High Fill Factor Polymer Solar Cells Incorporating a Low-Temperature Solution Processed $WO_3$ Hole Extraction Layer. *Adv. Energy Mater.* **2012**, *2*, 1433−1438.

(24) Tao, C.; Ruan, S. P.; Xie, G. H.; Kong, X. Z.; Shen, L.; Meng, F. X.; Liu, C. X.; Zhang, X. D.; Dong, W.; Chen, W. Y. Role of Tungsten Oxide in Inverted Polymer Solar Cells. *Appl. Phys. Lett.* **2009**, *94*, No. 043311.

(25) Irfan, I.; Turinske, A. J.; Bao, Z. N.; Gao, Y. L. Work Function Recovery of Air Exposed Molybdenum Oxide Thin Films. *Appl. Phys. Lett.* **2012**, *101*, No. 093305.

(26) Sun, Y. M.; Seo, J. H.; Takacs, C. J.; Seifter, J.; Heeger, A. J. Inverted Polymer Solar Cells Integrated with a Low-Temperature-Annealed Sol−Gel-Derived ZnO Film as an Electron Transport Layer. *Adv. Mater.* **2011**, *23*, 1679−1683.

(27) Hammond, S. R.; Meyer, J.; Widjonarko, N. E.; Ndione, P. F.; Sigdel, A. K.; Garcia, A.; Miedaner, A.; Lloyd, M. T.; Kahn, A.; Ginley, D. S.; Berry, J. J.; Olson, D. C. Low-Temperature, Solution-Processed Molybdenum Oxide Hole-Collection Layer for Organic Photovoltaics. *J. Mater. Chem.* **2012**, *22*, 3249−3254.

(28) Liu, F.; Shao, S.; Guo, X.; Zhao, Y.; Xie, Z. Efficient Polymer Photovoltaic Cells Using Solution-Processed $MoO_3$ as Anode Buffer Layer. *Sol. Energy Mater. Sol. Cells* **2010**, *94*, 842−845.




DOI: 10.1021/am509049t
*ACS Appl. Mater. Interfaces* 2015, 7, 7170−7179

(29) Murase, S.; Yang, Y. Solution Processed $MoO_3$ Interfacial Layer for Organic Photovoltaics Prepared by a Facile Synthesis Method. *Adv. Mater.* **2012**, *24*, 2459−2462.
(30) Zilberberg, K.; Gharbi, H.; Behrendt, A.; Trost, S.; Riedl, T. Low-Temperature, Solution-Processed $MoO_x$ for Efficient and Stable Organic Solar Cells. *ACS Appl. Mater. Interfaces* **2012**, *4*, 1164−1168.
(31) Jasieniak, J. J.; Seifter, J.; Jo, J.; Mates, T.; Heeger, A. J. A Solution-Processed $MoO_x$ Anode Interlayer for Use within Organic Photovoltaic Devices. *Adv. Funct. Mater.* **2012**, *22*, 2594−2605.
(32) Tan, Z. a.; Qian, D.; Zhang, W.; Li, L.; Ding, Y.; Xu, Q.; Wang, F.; Li, Y. Efficient and Stable Polymer Solar Cells with Solution-Processed Molybdenum Oxide Interfacial Layer. *J. Mater. Chem. A* **2013**, *1*, 657−664.
(33) Meyer, J.; Khalandovsky, R.; Gorrn, P.; Kahn, A. $MoO_3$ Films Spin-Coated from a Nanoparticle Suspension for Efficient Hole-Injection in Organic Electronics. *Adv. Mater.* **2011**, *23*, 70−73.
(34) Lee, Y. J.; Yi, J.; Gao, G. F.; Koerner, H.; Park, K.; Wang, J.; Luo, K. Y.; Vaia, R. A.; Hsu, J. W. P. Low-Temperature Solution-Processed Molybdenum Oxide Nanoparticle Hole Transport Layers for Organic Photovoltaic Devices. *Adv. Energy Mater.* **2012**, *2*, 1193−1197.
(35) Girotto, C.; Voroshazi, E.; Cheyns, D.; Heremans, P.; Rand, B. P. Solution-Processed $MoO_3$ Thin Films as a Hole-Injection Layer for Organic Solar Cells. *ACS Appl. Mater. Interfaces* **2011**, *3*, 3244−3247.
(36) Yang, T.; Wang, M.; Cao, Y.; Huang, F.; Huang, L.; Peng, J.; Gong, X.; Cheng, S. Z. D.; Cao, Y. Polymer Solar Cells with a Low-Temperature-Annealed Sol−Gel-Derived $MoO_x$ Film as a Hole Extraction Layer. *Adv. Energy Mater.* **2012**, *2*, 523−527.
(37) Sun, J.-Y.; Tseng, W.-H.; Lan, S.; Lin, S.-H.; Yang, P.-C.; Wu, C.-I.; Lin, C.-F. Performance Enhancement in Inverted Polymer Photovoltaics with Solution-Processed $MoO_x$ and Air-Plasma Treatment for Anode Modification. *Sol. Energy Mater. Sol. Cells* **2013**, *109*, 178−184.
(38) Ho, P.-Y.; Sun, J.-Y.; Kao, S.-H.; Kao, C.-Y.; Lin, S.-H.; Lan, S.; Tseng, W.-H.; Wu, C.-I.; Lin, C.-F. The Effects of $MoO_3$ Treatment on Inverted PBDTTT-C:$PC_{71}BM$ Solar Cells. *Sol. Energy Mater. Sol. Cells* **2013**, *119*, 235−240.
(39) Li, X. C.; Choy, W. C. H.; Xie, F. X.; Zhang, S. Q.; Hou, J. H. Room-Temperature Solution-Processed Molybdenum Oxide as a Hole Transport Layer with Ag Nanoparticles for Highly Efficient Inverted Organic Solar Cells. *J. Mater. Chem. A* **2013**, *1*, 6614−6621.
(40) Chang, Y. M.; Leu, C. Y. Conjugated Polyelectrolyte and Zinc Oxide Stacked Structure as an Interlayer in Highly Efficient and Stable Organic Photovoltaic Cells. *J. Mater. Chem. A* **2013**, *1*, 6446−6451.
(41) Stubhan, T.; Salinas, M.; Ebel, A.; Krebs, F. C.; Hirsch, A.; Halik, M.; Brabec, C. J. Increasing the Fill Factor of Inverted P3HT:PCBM Solar Cells through Surface Modification of Al-Doped ZnO Via Phosphonic Acid-Anchored $C_{60}$ SAMs. *Adv. Energy Mater.* **2012**, *2*, 532−535.
(42) Small, C. E.; Chen, S.; Subbiah, J.; Amb, C. M.; Tsang, S.-W.; Lai, T.-H.; Reynolds, J. R.; So, F. High-Efficiency Inverted Dithienogermole-Thienopyrrolodione-Based Polymer Solar Cells. *Nat. Photonics* **2012**, *6*, 115−120.
(43) Tan, M. J.; Wang, R.; Zhong, S.; Seah, K. Y.; Li, J.; Chen, Z.; Vijila, C.; Chen, W. ZnO:Polymer Composite Material to Eliminate Kink in *J*−*V* Curves of Inverted Polymer Solar Cells. *ECS Solid State Lett.* **2014**, *3*, Q9−Q12.
(44) Tiwari, J. P.; Pillai, S.; Parakh, S.; Ali, F.; Sharma, A.; Chand, S. A Futuristic Approach Towards Interface Layer Modifications for Improved Efficiency in Inverted Organic Solar Cells. *Appl. Phys. Lett.* **2014**, *104*, No. 041114.
(45) Liu, J.; Wu, J.; Shao, S.; Deng, Y.; Meng, B.; Xie, Z.; Geng, Y.; Wang, L.; Zhang, F. Printable Highly Conductive Conjugated Polymer Sensitized ZnO NCs as Cathode Interfacial Layer for Efficient Polymer Solar Cells. *ACS Appl. Mater. Interfaces* **2014**, *6*, 8237−8245.
(46) Kim, J.; Kim, H.; Kim, G.; Back, H.; Lee, K. Soluble Transition Metal Oxide/Polymeric Acid Composites for Efficient Hole-Transport Layers in Polymer Solar Cells. *ACS Appl. Mater. Interfaces* **2014**, *6*, 951−957.
(47) Lee, S. J.; Kim, B. S.; Kim, J.; Yusoff, A. R. B. M; Jang, J. Stable Organic Photovoltaic with PEDOT:PSS and $MoO_x$ Mixture Anode Interfacial Layer Without Encapsultation. *Org. Electron.* **2015**, *19*, 140−146.
(48) Xie, F. X.; Choy, W. C. H.; Wang, C. D.; Li, X. C.; Zhang, S. Q.; Hou, J. H. Low-Temperature Solution-Processed Hydrogen Molybdenum and Vanadium Bronzes for an Efficient Hole-Transport Layer in Organic Electronics. *Adv. Mater.* **2013**, *25*, 2051−2055.
(49) Li, W.; Hendriks, K. H.; Furlan, A.; Roelofs, W. S. C.; Wienk, M. M.; Janssen, R. A. J. Universal Correlation between Fibril Width and Quantum Efficiency in Diketopyrrolopyrrole-Based Polymer Solar Cells. *J. Am. Chem. Soc.* **2013**, *135*, 18942−18948.
(50) JPCDS No. 47-1320.
(51) Shao, S. Y.; Liu, J.; Bergqvist, J.; Shi, S. W.; Veit, C.; Wurfel, U.; Xie, Z. Y.; Zhang, F. L. In Situ Formation of $MoO_3$ in PEDOT:PSS Matrix: A Facile Way to Produce a Smooth and Less Hygroscopic Hole Transport Layer for Highly Stable Polymer Bulk Heterojunction Solar Cells. *Adv. Energy Mater.* **2013**, *3*, 349−355.
(52) Zhu, Y. W.; Yuan, Z. C.; Cui, W.; Wu, Z. W.; Sun, Q. J.; Wang, S. D.; Kang, Z. H.; Sun, B. Q. A Cost-Effective Commercial Soluble Oxide Cluster for Highly Efficient and Stable Organic Solar Cells. *J. Mater. Chem. A* **2014**, *2*, 1436−1442.
(53) Liu, J.; Shao, S. Y.; Fang, G.; Meng, B.; Xie, Z. Y.; Wang, L. X. High-Efficiency Inverted Polymer Solar Cells with Transparent and Work-Function Tunable $MoO_3$-Al Composite Film as Cathode Buffer Layer. *Adv. Mater.* **2012**, *24*, 2774−2779.
(54) Du, T. B.; Song, H. W.; Ilegbusi, O. J. Sol−Gel Derived ZnO/PVP Nanocomposite Thin Film for Superoxide Radical Sensor. *Mater. Sci. Eng., C* **2007**, *27*, 414−420.
(55) Battaglia, C.; de Nicolas, S. M.; De Wolf, S.; Yin, X. T.; Zheng, M.; Ballif, C.; Javey, A. Silicon Heterojunction Solar Cell with Passivated Hole Selective $MoO_x$ Contact. *Appl. Phys. Lett.* **2014**, *104*, No. 113902.
(56) Morandi, S.; Ghiotti, G.; Chiorino, A.; Comini, E. FT-IR and UV−vis−NIR Characterisation of Pure and Mixed $MoO_3$ and $WO_3$ Thin Films. *Thin Solid Films* **2005**, *490*, 74−80.
(57) Xia, Y. J.; Ouyang, J. Y. PEDOT:PSS Films with Significantly Enhanced Conductivities Induced by Preferential Solvation with Cosolvents and Their Application in Polymer Photovoltaic Cells. *J. Mater. Chem.* **2011**, *21*, 4927−4936.
(58) Friedel, B.; Brenner, T. J. K.; McNeill, C. R.; Steiner, U.; Greenham, N. C. Influence of Solution Heating on the Properties of PEDOT:PSS Colloidal Solutions and Impact on the Device Performance of Polymer Solar Cells. *Org. Electron.* **2011**, *12*, 1736−1745.
(59) White, M. S.; Olson, D. C.; Shaheen, S. E.; Kopidakis, N.; Ginley, D. S. Inverted Bulk-Heterojunction Organic Photovoltaic Device Using a Solution-Derived ZnO Underlayer. *Appl. Phys. Lett.* **2006**, *89*, No. 143517.
(60) Zhao, D. W.; Tan, S. T.; Ke, L.; Liu, P.; Kyaw, A. K. K.; Sun, X. W.; Lo, G. Q.; Kwong, D. L. Optimization of an Inverted Organic Solar Cell. *Sol. Energy Mater. Sol. Cells* **2010**, *94*, 985−991.
(61) Kyaw, A. K. K.; Wang, D. H.; Wynands, D.; Zhang, J.; Nguyen, T. Q.; Bazan, G. C.; Heeger, A. J. Improved Light Harvesting and Improved Efficiency by Insertion of an Optical Spacer (ZnO) in Solution-Processed Small-Molecule Solar Cells. *Nano Lett.* **2013**, *13*, 3796−3801.
(62) Meng, Y. H.; Hu, Z. H.; Ai, N.; Jiang, Z. X.; Wang, J.; Peng, J. B.; Cao, Y. Improving the Stability of Bulk Heterojunction Solar Cells by Incorporating PH-Neutral PEDOT:PSS as the Hole Transport Layer. *ACS Appl. Mater. Interfaces* **2014**, *6*, 5122−5129.
(63) Kumar, A.; Sista, S.; Yang, Y. Dipole Induced Anomalous S-Shape *I*−*V* Curves in Polymer Solar Cells. *J. Appl. Phys.* **2009**, *105*, No. 094512.


DOI: 10.1021/am509049t
*ACS Appl. Mater. Interfaces* 2015, 7, 7170−7179